ANALYSIS OF JOULE HEATING AND GENERALIZED SLIP FLOW IN FERROMAGNETIC NANOPARTICLES IN A CURVED CHANNEL USING CATTANEO-CHRISTOV HEAT FLUX THEORY

by

Zaheer ABBAS[a], Sifat HUSSAIN[a], Muhammad NAVEED[b*], Amir NADEEM[c], and Amjad ALI[d]

[a] Department of Mathematics, The Islamia University of Bahawalpur, Bahawalpur, Pakistan
[b] Department of Mathematics, Khwaja Fareed University of Engineering and Information Technology, Rahim Yar Khan, Pakistan
[c] Department of Mathematical Sciences, Federal Urdu University of Art, Science and Technology, Islamabad, Pakistan
[d] Centre for Advanced Studies in Pure and Applied Mathematics, Bahauddin Zakariya University, Multan, Pakistan

Original scientific paper
https://doi.org/10.2298/TSCI200410220A

This paper investigates the heat transport phenomenon by utilizing Cattaneo-Christov heat flux model on magnetic nanoparticles through a semi porous curved wall channel, incorporated with generalized slip condition and bent in a circle of radius, R_c. In addition, the energy equations takes into account the impacts of heat generation and Joule heating. To construct the flow model, a curvilinear co-ordinate scheme is used. The derived PDE are converted into system of ODE by incorporating appropriate similarity variables. Numerical simulation is used to achieve a numerical solution of the flow equations by using shooting technique. The influence of various parameters on temperature, rate of heat transfer, velocity and surface drag force are analyze and discussed in detail by using graphs and table. Also a well-known finite difference technique known as Keller box method is also used to verify and validate the obtained numerical results.

Key words: *ferromagnetic nanofluid, Cattaneo-Christov heat flux, heat generatio, generalized slip condition, semi-porous curved channel*

Introduction

The examination of nanofluid has attained immense attention received by the researchers due to the impact of nanotechnology in major industrial and engineering developments. The concept of the flow of nanofluid was initiated by Choi and Estman [1]. These types of liquids have diverse applications like, in power generators, thermal therapy for cancer treatment, hybrid-powered engines nuclear reactor, magnetic cell separation and magnetic drug targeting. The transport features of base fluid are enhanced by incorporating these nanoparticles to the base fluid. Several components that affect the thermal conductivity of the nanofluids are the shape and particle size, temperature, base fluid material and volume fraction [2]. The impact of

* Corresponding author, e-mail: rana.m.naveed@gmail.com

nanofluid in a flow caused by a stretching sheet was examined by Khan and Pop [3]. For more detailed information, the keen readers are advised of the articles [4-9] and references within.

Ferro fluid is a special type of nanofluid made up of magnetic nanoparticles. To ensure a steady suspension condition, ferrofluid with a diameter of 5-15 nm layered with some kind of wetting layer. Because of their small size these ferrofluids can quickly travel through a micro-channel without obstructing it act like a liquid molecule. These magnetic nanofluids are used in anode X-ray, energy conversion system, rotating generator, vacuum champers in a semi-conductor industry, viscous dampers for gravity, gradient satellites, in disk devices of a high speed computer to minimize the harmful dust particles and accelerometers. Sheikholeslami *et al.* [10] studied the applications of forced convection on ferrofluid as well as the consequences of the variable magnetic field. The different aspects of heat transmission in a MHD flow of ferrofluid across a stretchable cylinder with prescribed heat flux was reported by Qasim *et al.* [11]. Khan *et al.* [12] investigated the various features of hydromagnetic ferrofluid stagnation point flow towards a stretching sheet. Sheikholeslami and Ganji [13] investigated the problem of heat transport in ferrofluid-flow across a partial annulus enclosure with the magnetic field. The latest published literature specifies that many features for ferrofluid-flow have been discussed by researchers [14-18] and references in that.

The examination of transport phenomena including both mass and heat transmission has developed phenomenal popularity among many authors due to its widespread applications in engineering and manufacturing processes, such as food processing, power collector machinery and refrigeration. According to the study of the literature, several authors have used convectional models for the transmission of heat and mass, but these hypothesis are inadequate because of the significance of an infinite speed wave transfer. To reduce this problem thermal relaxation time and solutal are integrated. For the first time the thermal relaxation time was combined with Fourier's law by Cattaneo [19], resulting in perpendicular heat transmission. Later, Christov [20] improved the work was done by [19] by using higher convective Oldroyd differentiation rather than a partial time derivative. Hayat *et al.* [21] evaluates the double-diffusive model for viscoelastic nanoliquid in 3-D flow by using Cattaneo-Christov heat flux model. The characteristics of heat transport modelled with Cattaneo-Christov heat flux was inspected by Lieu *et al*. [22]. Farooq *et al.* [23] investigated the effects of heat transmission on the flow of squeezed fluid incorporated with Cattaneo-Christov heat flux model.

The influence of absorption and as well as heat generation on the convective heat flow problems received huge consideration due to its operation in cooling processes and solidification of costing. Aziz *et al.* [24] investigated numerically flow of nanofluid by a rotating disc with heat generation. Hosseinie *et al.* [25] have reported the effects of heat generation in existence of applied magnetic field on the nanofluid-flowing in a micro-channel. Sheikholeslami *et al.* [26] studied the result of heat generation and thermal diffusion on the flow of nanofluid over an oscillating plate.

The flow analysis in a narrow channel has attained much consequence because of its huge number of usages in the fields of engineering and biological procedure. Sajid *et al.* [27] examine the impacts heat transport on a ferrofluid-flow in a curved channel with Joule heating. The inspection of heat transfer phenomena by employing thermal radiation in a viscous fluid via a permeable curved channel was done Naveed *et al.* [28]. Lately, Abbas *et al.* [29] examined the Eyring-Powell fluid-flow in a curved channel. They modeled the energy equation incorporated with the Cattaneo-Christov heat transmission model.

In slip flow, the flow velocity at the firm wall remains non-zero, while in no-slip flow, the flow velocity at the firm wall is zero. The generalized slip condition, in which the slip length

is a component of shear stress was observed by Thompson and Troin [30]. Sajid *et al.* [31] solved numerically both planar and axisymmetric flow equations with generalized boundary slip condition. Several scholars have studied the impacts of generalized slip condition for Newtonian and non-Newtonian fluid for divers' geometries, see the articles [32-35].

The present study intends to assess the result of the applied magnetic field and heat generation on the ferrofluid over a curved channel. Also the generalized slip condition is imposed on the lower wall. Modelling of the heat equation is accomplished by considering Cattaneo-Christov heat flux model. Shooting technique is adopted to achieve the numerical solutions for the flow, pressure, skin friction coefficient, temperature, and the entire value of Nusselt number. Numerical results are displayed in tabular and graphical shapes.

Presentation of the problem

Consider a 2-D and an incompressible flow of a ferrofluid inside a curved channel. Let H be the width between the two curved walls of the channel. Also it is assumed that the upper wall of the channel is permeable and lower wall is rigid, fig. 1. Let us suppose that $\hat{T}_w$ be the temperature of the lower wall and $\hat{T}_0$ be the temperature of the upper wall with $\hat{T}_w > \hat{T}_0$. Let B_0 be the magnitude of the imposed magnetic field in r-direction. The consequences of the induced magnetic field are overlooked by considering low magnetic Reynolds theory. By aforesaid assumptions, the conservation laws for mass, momentum and energy equations formulated with Cattaneo-Christov heat flux theory with heat generation are given:

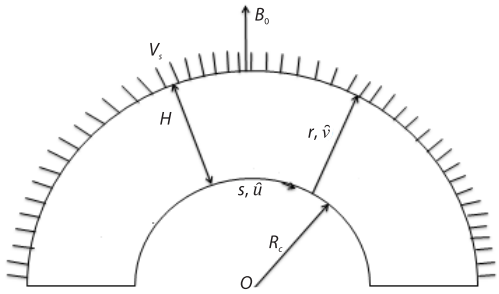

Figure 1. Physical model and co-ordinate system

$$R_c \frac{\partial \hat{u}}{\partial s} + \frac{\partial}{\partial r}\left\{\left(r + R_c\right)\hat{v}\right\} = 0 \tag{1}$$

$$\frac{1}{\rho_{\mathrm{nf}}}\frac{\partial p}{\partial r} = \frac{\hat{u}^2}{r + R_c} \tag{2}$$

$$\hat{v}\frac{\partial \hat{u}}{\partial r} + \frac{\hat{u}R_c}{r + R_c}\frac{\partial \hat{u}}{\partial s} + \frac{\hat{u}\hat{v}}{r + R_c} = -\frac{1}{\rho_{\mathrm{nf}}}\frac{R_c}{r + R_c}\frac{\partial p}{\partial s} + \frac{\mu_{\mathrm{nf}}}{\rho_{\mathrm{nf}}} \cdot \left[\frac{\partial^2 \hat{u}}{\partial r^2} - \frac{\hat{u}}{\left(r + R_c\right)^2} + \frac{1}{\left(R_c + r\right)}\frac{\partial \hat{u}}{\partial x}\right] - \frac{\sigma_{\mathrm{nf}} B_0^2 \hat{u}}{\rho_{\mathrm{nf}}} \tag{3}$$

$$\overline{v}\frac{\partial \hat{T}}{\partial r} + \frac{R_c \hat{u}}{\left(r + R_c\right)}\frac{\partial \hat{T}}{\partial s} + \phi_a \lambda_a = \alpha_{\mathrm{nf}}\left(\frac{\partial^2 \hat{T}}{\partial r^2} + \frac{1}{\left(r + R_c\right)}\frac{\partial \hat{T}}{\partial r}\right) + \frac{Q}{\left(\rho c_p\right)_{\mathrm{nf}}}\left(\hat{T} - \hat{T}_0\right) \tag{4}$$

where

$$\phi_a = \left\{\begin{array}{l} \dfrac{\hat{u}R_c^{\,2}}{\left(r + R_c\right)^2}\dfrac{\partial \hat{T}}{\partial s}\dfrac{\partial \hat{u}}{\partial s} + \dfrac{R_c \hat{u}}{\left(r + R_c\right)}\dfrac{\partial \hat{v}}{\partial s}\dfrac{\partial \hat{T}}{\partial r} + \dfrac{R_c \hat{v}}{\left(r + R_c\right)}\dfrac{\partial \hat{u}}{\partial r}\dfrac{\partial \hat{T}}{\partial s} + \overline{v}\dfrac{\partial \hat{v}}{\partial r}\dfrac{\partial \hat{T}}{\partial r} + \\ + \hat{v}^2\dfrac{\partial^2 \hat{T}}{\partial r^2} + \dfrac{2\hat{u}\hat{v}R_c}{\left(r + R_c\right)}\dfrac{\partial^2 \hat{T}}{\partial r \partial s}\dfrac{\hat{u}^2}{\left(R_c + r\right)^2}\dfrac{\partial^2 \hat{T}}{\partial s^2} - \dfrac{\hat{u}\hat{v}R_c}{\left(R_c + r\right)^2}\dfrac{\partial \hat{T}}{\partial s} \end{array}\right\}$$

In the previous equations, $\hat{u}$ and $\hat{v}$ are the part of velocity in s- and r-direction, also, Q, λ_a, $\hat{T}$, and p are the temperature-dependent volumetric rate of heat source, relaxation time of heat flux, temperature, and pressure of the fluid, respectively.

The viscosity of the nanoparticles [27] is given:

$$\mu_{\mathrm{nf}} = \frac{\mu_{\mathrm{f}}}{(1-\phi)^{2.5}} \tag{5}$$

where ϕ indicates the solid nanoparticles volume fraction.

The effective density, ρ_{nf}, thermal diffusivity, α_{nf}, heat capacitance, $(\rho c_p)_{\mathrm{nf}}$, and electrical conductivity of specific nanofluids are known:

$$\rho_{\mathrm{nf}} = \rho_{\mathrm{f}}(1-\phi) + \phi\rho_{\mathrm{s}} \tag{6}$$

$$\alpha_{\mathrm{nf}} = \frac{k_{\mathrm{nf}}}{(\rho c_p)_{\mathrm{nf}}} \tag{7}$$

$$(\rho c_p)_{\mathrm{nf}} = \phi(\rho c_p) + (1-\phi)(\rho c_p)_{\mathrm{f}} \tag{8}$$

$$\frac{\sigma_{\mathrm{nf}}}{\sigma_{\mathrm{f}}} = 1 + \frac{3\left(\frac{\sigma_{\mathrm{s}}}{\sigma_{\mathrm{f}}} - 1\right)\phi}{\left(2 + \frac{\sigma_s}{\sigma_{\mathrm{f}}}\right) - \phi\left(\frac{\sigma_{\mathrm{s}}}{\sigma_{\mathrm{f}}} - 1\right)} \tag{9}$$

In current study, we have adopted Maxwell [27] model to calculate the thermal conductivity of nanofluids restricted to spherical particles and is specified:

$$\frac{k_{\mathrm{nf}}}{k_{\mathrm{f}}} = \left[\frac{k_{\mathrm{s}} - 2\phi(k_{\mathrm{f}} - k_{\mathrm{s}}) + 2k_{\mathrm{f}}}{k_{\mathrm{s}} + \phi(k_{\mathrm{f}} - k_{\mathrm{s}}) + 2k_{\mathrm{f}}}\right] \tag{10}$$

In eqs. (5)-(10), the symbols s, f, and nf in the subscripts characterizes the thermophysical properties of nanosolid particles, base fluid and nanofluid, respectively, given in tab. 1.

Table 1. Thermophysical properties of water (base fluid) plus magnetite particles [27]

Properties	ρ [kgm^{-3}]	c_p [Jkgm^{-1}K^{-1}]	k [Wm^{-1}K^{-1}]	$\beta \cdot 10^5$ [K^{-1}]	σ [Ω^{-1}m^{-1}]
Base fluid/water	997.1	4179	0.613	21	0.05
Magnetic nano particles (Fe_3O_4)	5180	385	401	1.67	25000

According to Thompson and Troian [30], the generalized slip condition is given:

$$\hat{u}_t = \alpha_1\left(1 - \beta_1\frac{\partial\hat{u}}{\partial r}\right)^{-1/2}\frac{\partial\hat{u}}{\partial r}$$

where $\hat{u}_t$ is the tangential velocity, α_1 – the Navier's slip length, and β_1 – the reciprocal of critical shear rate.

The suitable boundary conditions:

$$\begin{aligned} &\hat{v} = 0,\ \hat{T} = \hat{T}_w,\ \hat{u} = U + \alpha_1(s)\left[1 - \beta_1(s)\tau_{rs}\right]^{-1/2}\tau_{rs} \ \text{ at } r = 0 \\ &\hat{v} = \frac{-V_s R_c}{r + R_c},\ \hat{u} = 0, \quad \hat{T} \to \hat{T}_0 \ \text{ as } r = H \end{aligned} \tag{11}$$

where $V_s < 0$ and $V_s > 0$, express the injection and suction.

For similar solution of the heat and flow equations are attained by taking the non-dimensional variables:

$$\hat{v} = \frac{-R_c V_s}{r + R_c} g(\eta),\ \hat{u} = \frac{Us}{H} g'(\eta),\ \eta = \frac{R_c}{H},\ p = P(\eta)\frac{\rho_f U^2 s^2}{H^2},\ \Theta(\eta) = \frac{\hat{T} - \hat{T}_0}{\hat{T}_w - \hat{T}_0} \tag{12}$$

Using eq. (12), continuity eq. (1) hold identically and eqs. (2)-(4) give way:

$$\frac{1}{\phi_2}\frac{\partial P}{\partial \eta} = \frac{g'^2}{\eta + C} \tag{13}$$

$$\frac{2C}{\phi_2(\eta + C)} P = \frac{\nu_{\mathrm{nf}}}{\mathrm{Re}\,\nu_{\mathrm{f}}}\left[g''' + \frac{g''}{\eta + C} - \frac{g'}{(\eta + C)^2} \right] - \frac{C}{\eta + C} g'^2 + \frac{C}{\eta + C} g g'' + \frac{C}{(\eta + C)^2} g g' - \frac{M \sigma_{\mathrm{nf}}}{\phi_2 \sigma_{\mathrm{f}}} g' \tag{14}$$

$$\Theta''\left[1 - \frac{k_{\mathrm{f}}}{k_{\mathrm{nf}}} \frac{\gamma \,\mathrm{Pr}\, \phi_3 C^2 g^2}{(\eta + C)^2} \right] + \frac{\Theta'}{\eta + C} + \mathrm{Pr}\,\phi_3 \frac{k_{\mathrm{f}}}{k_{\mathrm{nf}}}\left[\frac{\mathrm{Re}\, C g \Theta'}{\eta + C} - \frac{\gamma C^2 g g' \Theta'}{(\eta + C)^2} + \frac{\gamma C^2 g^2 \Theta'}{(\eta + C)^3} + \frac{\Lambda \Theta}{\phi_3} \right] = 0 \tag{15}$$

where

$$\mathrm{Pr} = \frac{\nu_{\mathrm{f}}}{\alpha_{\mathrm{f}}},\ C = \frac{R_c}{H},\ \mathrm{Re} = \frac{UH}{\nu_{\mathrm{f}}},\ M = \frac{\sigma_{\mathrm{f}} B_0^2 H}{\rho_{\mathrm{f}} U} \text{ and } \gamma = \frac{\lambda_a V_s^2}{\nu_{\mathrm{f}}}$$

are the Prandtl number, dimensionless radius of curvature, Reynolds number, magnetic or Hartmann number, thermal relaxation, and heat generation parameter correspondingly.

With boundary conditions:

$$g(0) = 0,\ \Theta(0) = 1,\ g'(0) = 1 + \lambda_1\left[1 + \lambda_2 \left\{ \frac{g'(0)}{C} - g''(0) \right\} \right]^{-1/2}\left[g''(0) - \frac{g'(0)}{C} \right]$$
$$g(1) = 1,\ \Theta(1) = 0,\ g'(1) = 0 \tag{16}$$

where

$$\lambda_1 = \frac{\alpha_1(s)U}{H^2},\ \lambda_2 = \frac{\beta_1(s)U}{H^2}$$

represents the velocity slip parameter and critical shear rate, respectively.

Excluding the pressure term from eqs. (13) and (14), we get:

$$g'''' + \frac{2g'''}{\eta + C} - \frac{g''}{(\eta + C)^2} + \frac{g'}{(\eta + C)^3} + \frac{\phi_1 C\,\mathrm{Re}}{\eta + C}(g g''' - g' g'') -$$
$$- \frac{\phi_1 C\,\mathrm{Re}}{(\eta + C)^2}(g'^2 - g g'') - \frac{\phi_1\,\mathrm{ReC}}{(\eta + C)^3} g g' - \frac{\sigma_{nf}\phi_1 M\,\mathrm{Re}}{\sigma_f \phi_2}\left(g'' + \frac{g'}{\eta + C} \right) = 0 \tag{17}$$

where

$$\phi_1 = (1 - \phi)^{2.5}\left[1 - \phi + \phi\left(\frac{\rho_s}{\rho_f} \right) \right],\ \phi_2 = 1 - \phi + \phi\left(\frac{\rho_{\mathrm{s}}}{\rho_{\mathrm{f}}} \right)$$
$$\phi_3 = 1 - \phi + \phi\frac{(\rho c_p)_{\mathrm{s}}}{(\rho c_p)_{\mathrm{f}}},\ \phi_4 = (1 - \phi)^{2.5}\left[1 - \phi + \phi\frac{(\rho c_p)_{\mathrm{s}}}{(\rho c_p)_{\mathrm{f}}} \right] \tag{18}$$

The fluid velocity $g(\eta)$ is obtain from eq. (17) and then the pressure of the fluid can be determined by eq. (14).

The expression for the heat transfer rate and the skin frictionwards the s-direction are given:

$$C_{\mathrm{f}} = \frac{\tau_{rs}}{\rho_{\mathrm{nf}} U_w^2},\ \mathrm{Nu}_s = \frac{q_w s}{\left(\hat{T}_w - \hat{T}_0\right) k_{\mathrm{f}}} \tag{19}$$

where τ_{rs} and q_w are the wall shear stress and the heat flux which are given:

$$q_w = -k_{\mathrm{nf}} \left.\frac{\partial \hat{T}}{\partial r}\right|_{r=o},\ \tau_{rs} = \mu_{\mathrm{nf}} \left.\left(\frac{\partial \hat{u}}{\partial r} - \frac{\hat{u}}{r + R_c}\right)\right|_{r=0} \tag{20}$$

Therefore, for the non-dimensional variables, eq. (19) become:

$$\mathrm{Re}_s^{1/2} C_f = \frac{1}{\phi_1}\left[g''(0) - \frac{g'(0)}{C}\right] \tag{21}$$

$$\mathrm{Re}_s^{-1/2} \mathrm{Nu}_s = -\frac{k_{\mathrm{nf}} \Theta(0)}{k_{\mathrm{f}}} \tag{22}$$

where $\mathrm{Re}_s = as^2/\nu_{\mathrm{f}}$ is the points the local Reynold number.

Results and discussion

The non-linear boundary value problem which is composed of eqs. (15) and (17) as well as the boundary conditions (16) are solved numerically by using shooting method to determine the influence of the relevant parameters such as magnetic parameter, M, slip parameters, λ_1 and λ_2, dimensionless radius of curvature, C, solid volume fraction, ϕ, Eckert number, and Reynolds number, on fluid velocity $g'(\eta)$, temperature, $\Theta(\eta)$, and pressure $P(\eta)$. In addition, the impacts of aforesaid parameters on skin friction coefficient $\mathrm{Re}_s^{1/2} C_{\mathrm{f}}$ and the rate of heat transfer $\mathrm{Re}_s^{-1/2} \mathrm{Nu}_s$ are also plotted through graphs and table.

By keeping the other parameters fixed, fig. 2 is represents the influence of Hartmann's number, M, on velocity field $g'(\eta)$. For higher values of M, the fluid velocity is reduced but $\eta = 0.5$ it begins to increase. This is because that the magnetic field acts as an opposing force. Figure 3 represents the effects of solid volume fraction, ϕ, on $g'(\eta)$. The velocity field diminishes with an increase in ϕ but it has opposite behavior after $\eta = 0.5$. The impact of slip parameter λ_1 on $g'(\eta)$ is presented in fig. 4. It can be deduced that as λ_1 increases, the fluid velocity initially reduces but it has opposite trend after $\eta = 0.5$. The influence of critical shear rate λ_1 on $g'(\eta)$ is

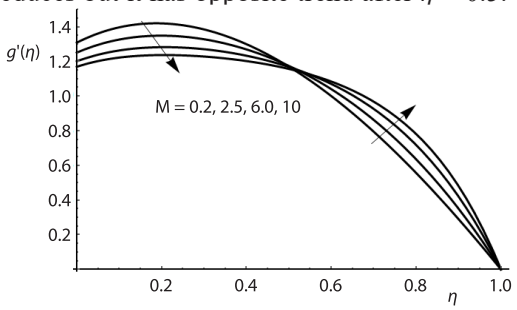

Figure 2. Effect of M on $f'(\eta)$ when $\phi = 0.03$, $\lambda_2 = 0.3$, $\lambda_1 = 0.4$, Re = 4, and $C = 8$

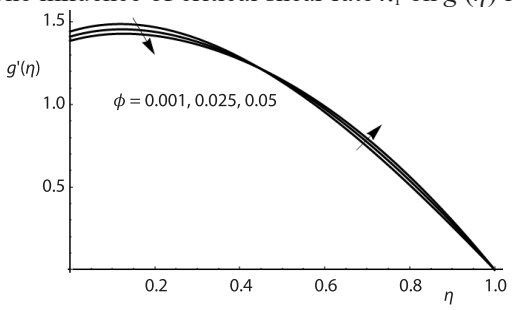

Figure 3. Effect of ϕ on $f'(\eta)$ when Re = 8, $\lambda_1 = 0.9$, M = 6, $\lambda_2 = 0.2$, and $C = 10$

displayed in fig. 5. It is noticed that a similar behavior is observed for λ_2 as for the parameter λ_1. Figure 6 depicts the influence of dimensionless radius of curvature, C, on $g'(\eta)$ by keeping the other parameters fixed. The fluid velocity $g'(\eta)$ is decreased for higher values of C but after $\eta = 0.5$ it starts increasing. The effect of Reynolds number on $g'(\eta)$ is presented in fig. 7. It can be seen from this figure that for higher values Reynolds number, the fluid velocity reduces but after $\eta = 0.5$ the consequence is opposite.

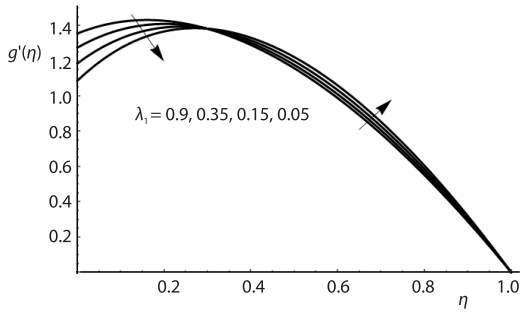

Figure 4. Effect of λ_1 on $f'(\eta)$ when Re = 2, $\phi = 0.03$, M = 0.5, $\lambda_1 = 0.2$, and $C = 3$

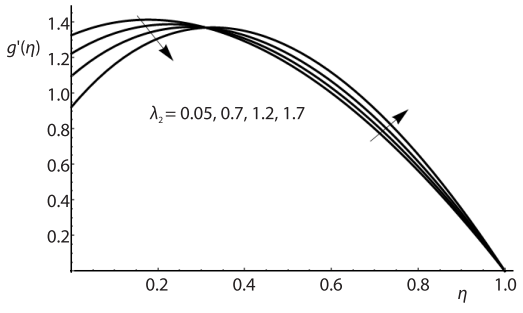

Figure 5. Effects of λ_2 on $f'(\eta)$ when M = 0.5, Re = 1, $\phi = 0.03$, $\lambda_1 = 0.6$, and $C = 3$

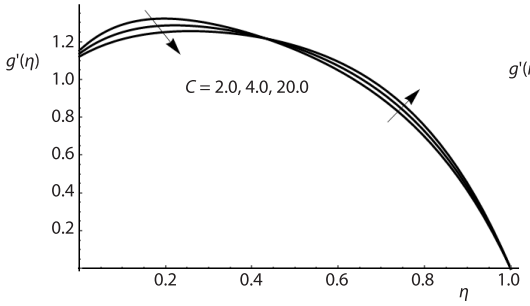

Figure 6. Effect of C on $f'(\eta)$ when $\lambda_2 = 0.05$, $\phi = 0.04$, M = 6, $\lambda_1 = 0.1$, and Re = 5

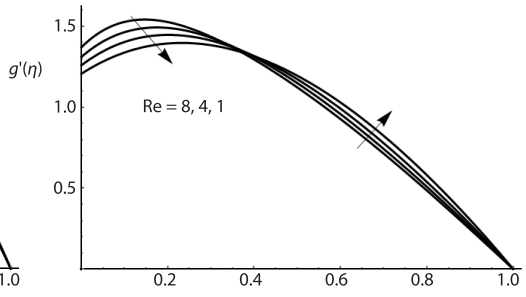

Figure 7. Effect of Re on $f'(\eta)$ when $\lambda_2 = 0.1$, $\phi = 0.05$, M = 0.2, $\lambda_1 = 0.2$, and $C = 2$

Figure 8 represents the effects of λ_1 and M on pressure distribution $P(\eta)$. For upper values of M the pressure distribution increases but it reduces for developed values of λ_1. Figure 9 depicts the change in $P(\eta)$ for diverse values of dimensionless C and solid volume fraction, ϕ. The $P(\eta)$ rises with an increment in ϕ, however it is reduced for upper values of C. The variation

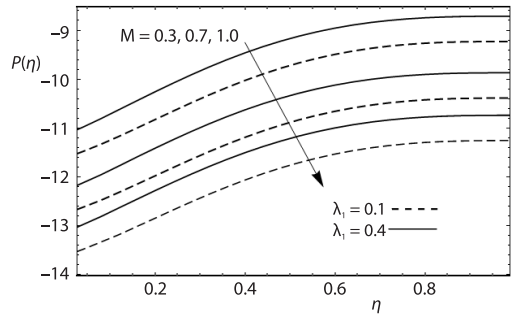

Figure 8. Impact of M and λ_1 on $P(\eta)$ when $\lambda_2 = 0.3$, $C = 2$, Re = 4, and $\phi = 0.03$

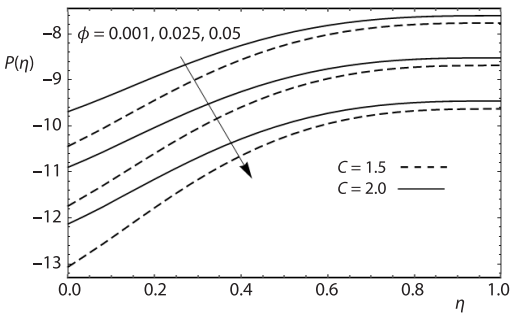

Figure 9. Effects of ϕ and K_1 on $P(\eta)$ when $\lambda_2 = 0.3$, $\lambda_1 = 0.4$, Re = 4, and M = 0.3

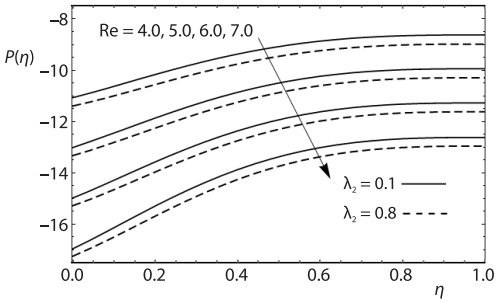

Figure 10. Effects of Re and λ_2 on $P(\eta)$ when $\phi = 0.03$, $\lambda_1 = 0.4$, $C = 2$, and M = 0.3

in $P(\eta)$ for different values of λ_2 and Reynolds number is shown in fig. 10. It is observed that $P(\eta)$ increases for higher values of Reynolds number, however it is reduced with an increase in λ_2.

Figure 11. represents the effect of ϕ on temperature distribution, $\Theta(\eta)$. It is noticed by this figure that the temperature of the fluid is increased for higher values of ϕ. Figure 12 represents the impact of heat generation parameter, Λ, on $\Theta(\eta)$. This figure displays that for upper values of Λ results in an increase in the temperature of the fluid. The impact of M and Eckert number on $\Theta(\eta)$ is shown in fig. 13. It is evident from this figure that $\Theta(\eta)$ is increased for both the M and Eckert number. Figure 14 represents the influence of thermal relaxation parameter, γ, on $\Theta(\eta)$. A decrease in the temperature distribution is observed with an increase in the values of γ. Figure 15 shows the change in $\Theta(\eta)$ for diverse values of Prandtl number. It is observed that $\Theta(\eta)$ decreases with an increase in Prandtl number. The physical argument of this behavior is that the rate of thermal diffusion reduces with a rise in Prandtl number. The effects of Reynolds number on $\Theta(\eta)$ is shown in fig. 16. It can be seen from this graph that $\Theta(\eta)$ is reducing for developed values of Reynolds number.

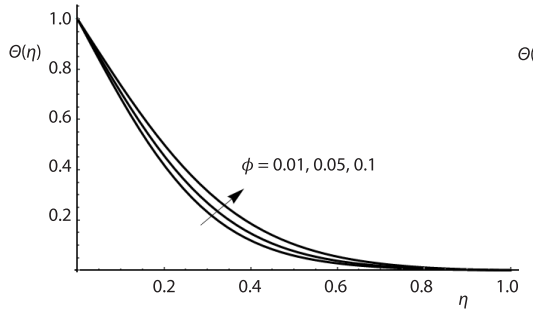

Figure 11. Impact of ϕ on $\Theta(\eta)$ when M = 0.5, Re = 4, $\lambda_1 = 0.6$, $\lambda_2 = 0.05$, $C = 2$, $\Lambda = 0.2$, Pr = 4, Ec = 0.1, and $\gamma = 0.2$

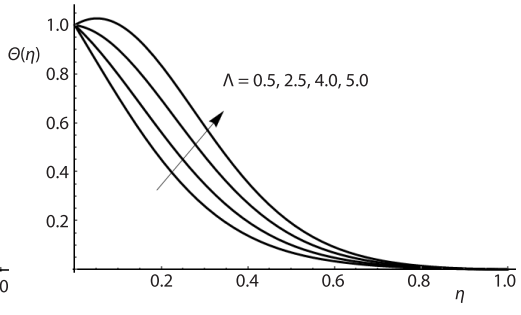

Figure 12. Impact of Λ on $\Theta(\eta)$ when M = 0.5, $\phi = 0.03$, Re = 4, $\lambda_1 = 0.6$, Ec = 0.1, $\lambda_2 = 0.05$, $C = 2$, Pr = 4, and $\gamma = 0.1$

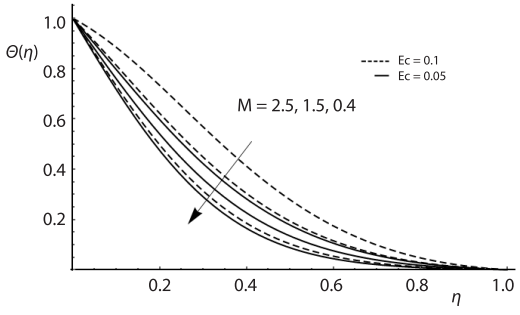

Figure 13. Impact of M and Ec on $\Theta(\eta)$ when $\phi = 0.05$, Re = 4, $\lambda_1 = 0.6$, $\lambda_2 = 0.5$, $\gamma = 0.1$, Pr = 3, $C = 2$, and $\Lambda = 0.1$

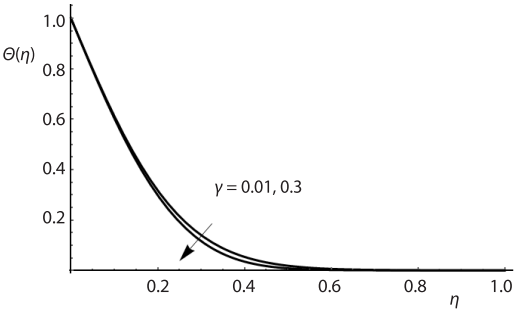

Figure 14. Impact of γ on $\Theta(\eta)$ when M = 0.3, $\phi = 0.05$, Re = 5, $\lambda_1 = 0.6$, $\lambda_2 = 0.5$, Pr = 4.5, $C = 2$, Ec = 0.01, and $\Lambda = 0.2$

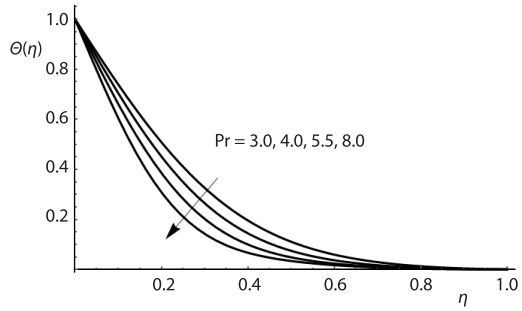

Figure 15. Effects of Pr on Θ(η) when M = 0.5, ϕ = 0.05, Re = 4, λ_1 = 0.6, λ_2 = 0.05, C = 2, Ec = 0.1, γ = 0.1, and Λ = 0.1

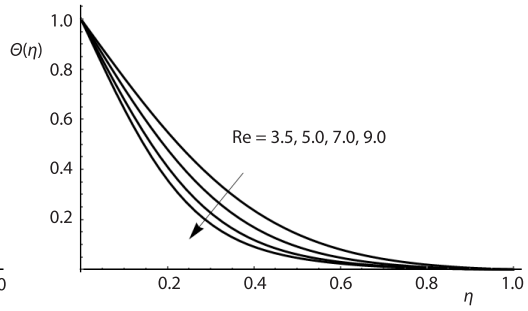

Figure 16. Impact of Re on Θ(η) when Pr = 3, C = 2, Ec = 0.1, M = 0.6, λ_1 = 0.6, ϕ = 0.05, Λ = 0.2, and γ = 0.1

Figure 17 gives the change in the skin friction coefficient $\mathrm{Re}_s^{-1/2}C_f$ *vs*. λ_1 with diverse values of λ_2 . It is evident from this graph that an increase in λ_1, results in decrease in absolute values of $\mathrm{Re}_s^{-1/2}C_f$, however the effect is opposite for the parameter λ_2. The variation in the $\mathrm{Re}_s^{-1/2}C_f$ via M for different values of ϕ is represent in fig. 18. It is noticed that for higher values ϕ, results in an increases in $\mathrm{Re}_s^{-1/2}C_f$ but it has the opposite behavior for M.

Table 2 gives the change in the local Nusselt number Θ(η) for different parameters. It is witnessed by this table that for higher values of Λ, M, Eckreman number, Reynolds nimber, γ, and Prandtl number, the magnitude of Θ(η) decreases, however it increases with an increase in ϕ.

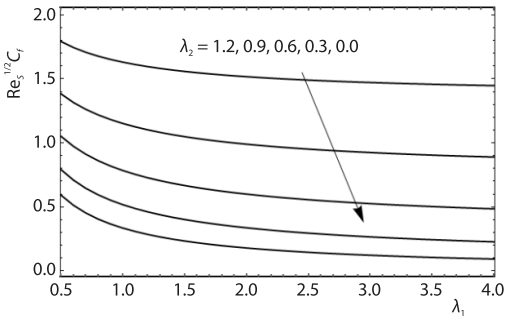

Figure 17. Impact of λ_2 *vs*. λ_1 on $\mathrm{Re}_s^{-1/2}C_f$ when ϕ = 0.04, M = 2, re = 3, and C = 2

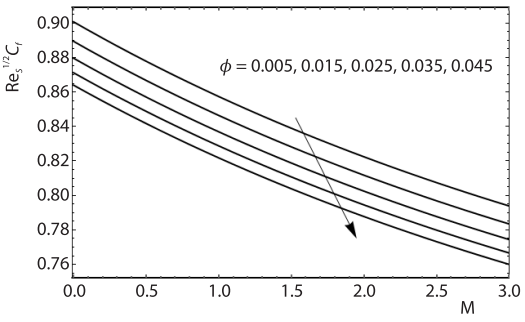

Figure 18. Effects of ϕ *vs*. M on $\mathrm{Re}_s^{-1/2}C_f$ when λ_2 = 0.3, λ_1 = 0.5, Re = 3, and C = 2

Conclusions

In this article, we have investigated heat transfer and flow of ferro fluid via a permeable curved channel with generalized boundary slip condition. Obtained numerical results are also validated by a finite difference scheme known as Kellar-box method. The effects of thermal relaxation, Joule heating and heat generation parameters in energy equation are also discussed. The shooting method is adopted to determine the numerical solutions for different flow parameters for velocity, temperature, rate of heat transfer, pressure and drag surface force. In this analysis following major outcomes were observed as follows.

- The fluid velocity decreases as radius of curvature, C, solid volume fraction, ϕ, magnetic parameter, Reynold number, slip parameters λ_1 and λ_2 increase.

Table 2. Numerical values of Θ(η) for different Reynolds number, magnetic parameter, Eckert number, Prandtl number, Λ, and γ by keeping $C = 2$, $\lambda_1 = 0.7$, and $\lambda_2 = 0.4$ fixed

Re	M	ϕ	Pr	Λ	γ	Ec	Shooting method Θ(η)	Kellar box method Θ(η)
0.5	0.6	0.1	2.0	0.5	0.2	0.5	1.08911	1.08911
1.5							0.83251	0.83251
2.0							0.71582	0.71582
2.5							0.60576	0.60576
2.0	0.2						1.65549	1.65549
	0.5						0.94982	0.94982
	0.7						0.48240	0.48240
	0.9						0.01729	0.01729
	0.6	0.15					0.71496	0.71496
		0.2					0.72310	0.72310
		0.25					0.74127	0.74127
		0.3					0.77075	0.77075
		0.1	1.5				0.93372	0.93372
			2.5				0.50990	0.50990
			3.0				0.31669	0.31669
			3.5				0.13616	0.13616
			2.0	0.1			0.73566	0.73566
				0.2			0.71582	0.71582
				0.3			0.69662	0.69662
				0.4			0.67835	0.67835
				0.2	0.2		0.93150	0.93150
					0.4		0.78910	0.78910
					0.6		0.64107	0.64107
					1.0		0.32612	0.32612
					0.5	0.1	1.84247	1.84247
						0.3	1.27915	1.27915
						0.5	0.71582	0.71582
						0.7	0.15250	0.15250

- The magnitudes of pressure distribution are enhanced for larger values of M, Reynolds number, and ϕ, however it decreases with an rise in the parameters λ_1, C, and λ_2.
- According to the results of this analysis, the temperature field is improved for upper values of Λ and ϕ. The temperature profile on the other hand, shows a decrease as the values of Prandtl and Reynold numbers, and γ rise.
- For larger values of λ_2 the skin friction coefficient is increased, but it progressively decreases for the parameters ϕ, λ_1, and M.
- For increasing the values γ and Λ, the Nusselt number reduces. Though, it has an opposite behavior for Prandtl and Reynolds numbers, and ϕ.

References

[1] Choi, S. U. S., Estman, J. A., Enhancing Thermal Conductivity of Fluids with Nanoparticles, *ASME-Fed*, *231* (1995), Jan., pp. 99-106
[2] Ozerinc, S., *et al.*, Enhanced Thermal Conductivity of Nanofluids: A State-of-the-Art Review, *Micro-Fluidics Nanofluidics*, *8* (2010), 2, pp. 145-175
[3] Khan, W. A., Pop, I., Boundary-Layer Flow of a Nanofluid Past a Stretching Sheet, *Int. J. Heat Mass Transf.*, *53* (2010), 11-12, pp. 2477-2483
[4] Vajravelu, *et al*., The Effect of Variable Viscosity on the Flow and Heat Transfer of a Viscous Ag-Water and Cu-Water Nanofluids, *Journal Hydro*, *25* (2013), 1, pp. 1-9
[5] Hatami, M., *et al*., Heat Transfer and Flow Analysis of Nanofluid-Flow between Parallel Plates in Presense of Variable Magnetic Field Using HPM, *Journal Mage. Magn. Mater*., *396* (2015), Aug., pp. 275-282
[6] Hasnain. J., Abbas. Z., Entropy Generation Analysis on Two-Phase Micropolar Nanofluids Flowin an Inclined Channel with Convective Heat Transfer, *Thermal Science*, *23* (2019), 3, pp. 1765-1777
[7] Abbas, Z., *et al*., Hydromagnetic Slip Flow of Nanofluid over a Curved Stretching Surface with Heat Generation, *Journal Molec. Liqu*., *215* (2016), 1, pp. 756-765
[8] Khan, M., *et al*., Numerical Study of Unsteady Axisymmetric Flow and Heat Transfer in Carreay Fluid Past a Stretched Surface, *Thermal Science*, *22* (2018), 6B, pp. 2859-2869
[9] Najib, N., *et al*., Dual Solutions of Boundary-Layer Flow over a Moving Surface in a Flowing Nanofluid with Second Order Slip, *Thermal Science*, *24* (2020), 2, pp. 1117-1129
[10] Sheikholeslami, M., *et al*., Forced Convection Heat Transfer in a Semi Annulus under the Influence of a Variable Magnetic Field, *Int. J. Heat Mass Transf*., *92* (2016), Jan., pp. 339-348
[11] Qasim, M., *et al*., The MHD Boundary-Layer Slip Flow and Heat Transfer of Ferrofluid along a Stretching Cylinder with Prescribed Heat Flux, *Plos One*, *9* (2014), 1, e83930
[12] Khan. A., *et al*., The MHD Stagnation Point Ferrofluid-Flow and Heat Transfer Towards a Stretching Sheet, *IEE Trans, Nanotech*., *13* (2014), 1, pp. 35-40
[13] Sheikholeslami, M., Ganji, D. D., Ferrohydrodynamic and Magnetohydrodynamic Effects on Ferrofluid-Flow and Convective Heat Transfer, *Energy*, *75* (2014), Oct., pp. 400-410
[14] Abbas, Z., Sheikh, M., Numerical Study of Homogeneous-Heterogeneous Reactions on Stagnation Point Flow of Ferrofluid with Non-Linear Slip Condition, *Chi. J .Chem. Eng*., *25* (2017), 1, pp. 11-17
[15] Yang, S., *et al*., The Effects of Uniform Magnetic Field on Spatial-Temporal Evaluations of Thermo Capillary Convection with the Silicon Oil Base Ferrofluid Fluid, *Thermal Sciience*, *24* (2020), 6B, pp. 4159-4171
[16] Abbas. Z., Hasnain, J., Two-Phase Magnetoconvection Flow of Magnetite Nanoparticles in a Horizontal Composite Porous Annulus, *Resu. Phys*., *7* (2017), Dec., pp. 574-580
[17] Ibrahim, A., Kayfeci, M., Comparative Analysis of a Solar Three Generation Based on Parabolic through Collectors Using Graphene and Ferrofluid Nanoparticles, *Thermal Science*, *25* (2021), 4A, pp. 2549-2563
[18] Goharkhah, M., Ashjaee, M., Effect of an Alternating Non-Uniform Magnetic Field on Ferrofluid-Flow and Heat Transfer in a Channel, *Journal Magn. Magn. Mater*., *362* (2014), C, pp. 80-89
[19] Cattaneo, C., Sulla conduzionedelcalore (in Italian), *Atti Sem Mat Fis Uni Modena*, *3* (1948), pp. 83-101
[20] Christov, C. I., On Frame Indifferent Formulation of the Maxwell-Cattaneo Model of Finite-Speed Heat Conduction, *Mec. Resear, Comm*., *36* (2009), 4, pp. 481-486
[21] Hayat, T., *et al*., Cattaneo-Christov Double-Diffusion Theory for 3-D Flow of Viscoelastic Nanofluid with the Effect of Heat Generation/Absorption., *Res. Phys.*, *8* (2018), Mar., pp. 489-195
[22] Liu, L., *et al*., Heat Conduction with Fractional Cattaneo-Christov Upper-Convective Derivative Flux Model, *Int. J. Eng. Sci.*, *112* (2017), Feb., pp. 421-426
[23] Farooq. M., *et al*., Analysis of Cattaneo-Christov Heat and Mass Fluxes in the Squeezed Flow Embedded in Porous Medium with Variable Mass Diffusivity, *Res. Phys*., *7* (2017), Sept., pp. 3788-3796
[24] Aziz. A., *et al*., Numerical Study of Heat Generation/Absorption in Flow of Nanofluid by a Rotating Disk, *Res. Phys*., *8* (2018), Mar., pp. 785-792
[25] Hosseini, S. R., *et al*., Entropy Analysis of Nanofluid Convection in a Heated Porous Micro-Channel under MHD Field Considering Solid Heat Generation, *Powd. Tech*., *344* (2019), Dec., pp. 914-925
[26] Sheikholeslami, M., *et al*., Effect of Thermal Diffusion and Heat Generation on MHD Nanofluid-Flow Past on Oscillating Vertical Plate through Porous Medium, *Journal Mol. Liq*., *257* (2018), Feb., pp. 12-25
[27] Sajid, M., *et al*., Joule Heating and Magnetohydrodynamics Effects on Ferrofluid-Flow in a Semi Porous Curved Channel, *Journal Mol. Liq*., *222* (2016), Oct, pp. 1115-1120
[28] Naveed, M., *et al*., Flow and Heat Transfer in a Semiporous Curved Channel with Radiation and Porosity Effects, *Journal Por. Med*., *19* (2016), 5, pp. 379-389

[29] Abbas, Z., *et al*., Analysis of Eyring-Powell Liquid-Flow in Curved Channel with Cattaneo-Christov Heat Flux Model, *Journal Braz. Soci. Mech. Sci. Eng*., *40* (2018), 8, 90
[30] Thompson, P. A., Troian, S. M., A General Boundary Condition for Liquid-Flow at Solid Surfaces, *Nature*, *389* (1997), 6649
[31] Sajid, M., *et al*., Stretching Flows with General Slip Boundary Condition, *Int. J. Mod. Phys. B*., *24* (2010), 30, pp. 5939-5947
[32] Abbas, Z., Sheikh, M., Numerical Study of Homogeneous-Heterogeneous Reactions on Stagnation Point Flow of Ferrofluid with Non-Linear Slip Condition, *Chi. J. Chem. Eng*., *25* (2017), 1, pp. 11-17
[33] Abbas, Z., *et al*., Stagnation-Point Flow of a Hydromagnetic Viscous Fluid over Stretching/Shrinking Sheet with Generalized Slip Condition in the Presence of Homogeneous-Heterogeneous Reactions, *Journal Taiw. Instit. Chem. Eng*., *55* (2015), Oct., pp. 69-75
[34] Salahuddin, T., *et al*., Carreau Nanofluid Impinging over a Stretching Cylinder with Generalized Slip Effects: Using Finite Difference Scheme, *Res. Phys*., *7* (2017), pp. 3090-3099
[35] Azese, M. N., On the Generalization of Velocity Slip in Fluid-Flows Using a Steady-State Series Expansion of the Wall Shear Stress: Case of Simple Newtonian Fluids, *Euro. J. Mech. B/Fluid*, *57* (2016), May-June, pp. 204-213

Paper submitted: April 10, 2020
Paper revised: May 4, 2021
Paper accepted: May 17, 2021